Numerical validation of the Wiener-Hopf approach

Numerical validation of the Wiener-Hopf approach to wedge problems

G. Lombardi*

Abstract – **This paper shows the capabilities of the Wiener-Hopf technique to solve arbitrary impenetrable wedge problems. In particular the reduction of factorization problem to a Fredholm equation provides very accurate and efficient numerical results using simple quadrature techniques.**

1 INTRODUCTION

Fig. 1 illustrates the problem of the diffraction by a plane wave at skew incidence on an impenetrable wedge immersed in a medium with permettivity ε and permeability μ.

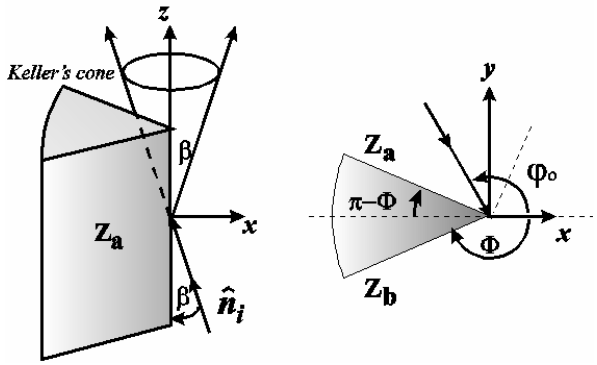

Fig.1: geometry of the problem

Using the reference system, the parameters, the formulation and the procedure presented in [1] we obtain the following Classic Wiener-Hopf equation in $\overline{\eta} - plane$:

$$\overline{G}(\overline{\eta})\overline{X}_{+}(\overline{\eta}) = \overline{X}_{-}(\overline{\eta}) \qquad (1)$$

where $\overline{G}(\overline{\eta})$ is a matrix kernel, and $\overline{X}_{+}(\overline{\eta})$, $\overline{X}_{-}(\overline{\eta})$ are the plus and minus unknown functions defined in [1] and referred to the field components along the $\varphi = 0, \pm\Phi$ directions.

Using the Cauchy decomposition formula we obtain that the factorization problem for the plus unknown and for the plus factorized matrix can be reduced to a Fredholm integral equation of second kind [1]:

$$\overline{G}(\overline{\eta})X_{i+}(\overline{\eta}) + \frac{1}{2\pi j}\int_{-\infty}^{\infty}\frac{\left[\overline{G}(x)-\overline{G}(\overline{\eta})\right]X_{i+}(x)}{x-\overline{\eta}}dx = \frac{R_i}{\overline{\eta}-\overline{\eta}_p} \qquad (2)$$

However the numerical evaluation of (2) shows slow convergence, therefore we introduce spectral transformations to obtain formulations with a superior rate of convergence.

2 SOLUTION OF THE FREDHOLM EQUATION

2.1 Complex plane transformations and contour warp for equation (2)

We introduce the $w - plane$ and the $\overline{w} - plane$ defined through the following equations:

$$\overline{\eta} = -\tau_o \cos\overline{w},\ \eta = -\tau_o \cos w,\ \ w = \frac{\Phi}{\pi}\overline{w} \qquad (3)$$

The introduction of $w-$ and $\overline{w} - plane$ is important to evaluate the far field in terms of the Wiener-Hopf solution by using the standard procedure based on Sommerfeld functions, see for example [2].
We observe that the kernel components of eq. (2) provide slow numerical convergence for the integration in $\overline{\eta} - plane$ and $\overline{w} - plane$, thus it is not possible to apply simple quadrature scheme for the numerical solution.
By analyzing the kernel properties we define the transformation $\overline{w} = -\pi/2 + jt$ which corresponds to warp the contour path constituted by the real axis into the straight line λ_α that joins the points $-j\,\tau_o$ and $j\,\tau_o$, see Fig.2.

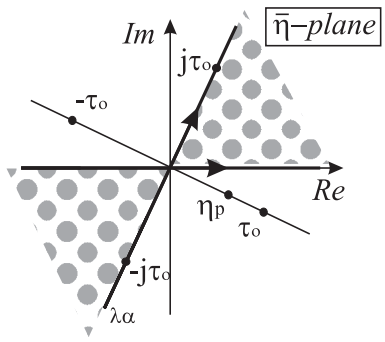

Fig.2: The contour path λ_α in the $\overline{\eta} - plane$

In the $\overline{w} - plane$ the contour λ_α is mapped into the contour $\lambda_{\overline{w}}$, see Fig. 3. Besides Fig. 3 shows the image of the proper sheet and improper sheet of the

Dipartimento di Elettronica, Politecnico di Torino, C.so Duca degli Abruzzi 24, 10129 Torino, Italy. Email: guido.lombardi@polito.it

$\bar{\eta} - plane$ onto the $\bar{w} - plane$ respectively with light gray colors and dark gray colors. For the proper sheet, the images of four quadrant 1, 2, 3 and 4 are limited by the images of the standard branch lines labelled with $b_{\pm\bar{w}}$. The $r_{\bar{w}}$ and $i_{\bar{w}}$ lines are the images of the real and imaginary axes of $\bar{\eta} - plane$. In the figure τ_o is equal to *1-j 0.1*.

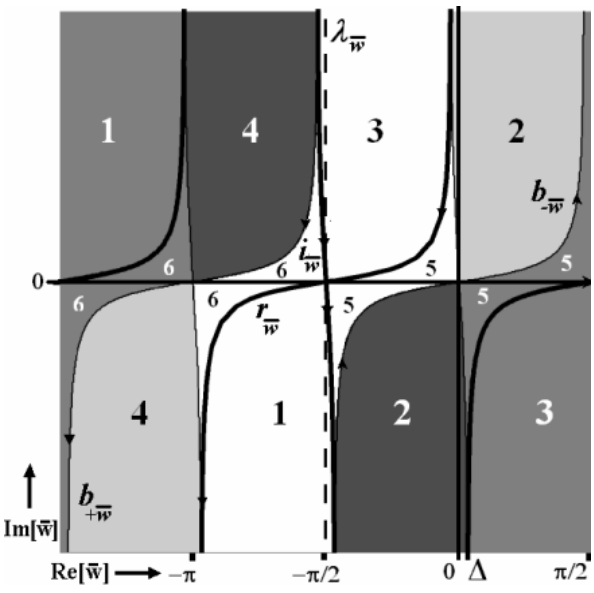

Fig.2: The contour path $\lambda_{\bar{w}}$ in the $\bar{w} - plane$

2.2 Numerical evaluation of equation (2)

By integrating along the contour $\lambda_{\bar{w}}$ and with reference to the quantities defined in [1] equation (2) becomes:

$$H(t)Y_i(t) + \frac{1}{2\pi j}\int_{-\infty}^{+\infty} m(t,u)Y_i(u)du = -\frac{R_i}{\tau_o(j\sinh t - \cos\bar{w}_p)}, \quad (4)$$

where the *m(t,u)* is defined in [1].

We obtain the following linear system using simple quadrature schemes for Fredholm equations:

$$H(hr)Y_{ia}(hr) + \frac{h}{2\pi j}\sum_{s=-A/h}^{A/h} m(hr,hi)Y_{ia}(hs) = -\frac{R_i}{\tau_o(j\sinh hr - \cos\bar{w}_p)}, \quad (5)$$

where $r = 0, \pm1, \pm2, ..., \pm A/h$ and *h* has to be chosen as small as possible and A has to be chosen as large as possible.

The solution of the previous equations yields the representation of the functions $X_{i+}(\bar{\eta}) = \hat{X}_{i+}(w)$, (6). Representation (6) holds only on the strip $-\Phi \le \mathrm{Re}[w] \le 0$, thus we need to extend analytically the validity of the numerical solution in the whole *w-plane*, as described in [1].

By using the Sommerfeld functions and the UTD theory we can obtain expression of the far fields [1]-[3].

$$\hat{X}_{ia+}(w) = -\frac{\hat{G}(w)^{-1}}{2\pi j}h\sum_{s=-A/h}^{A/h} m[-j(\frac{\pi}{\Phi}w + \frac{\pi}{2}), hs]\,Y_{ia}(hs) + \hat{G}(w)^{-1}\frac{R_i}{\tau_o(\cos\bar{w}_p - \cos\frac{\pi}{\Phi}w)}, \quad (6)$$

3 CONVERGENCE PROPERTIES

In this section, for the sake of simplicity, we refer to the isotropic impedance wedge at normal incidence in order to analyze and describe the properties of the Fredholm integral equation (2).

In the case of $\alpha_o = 0$ (normal incidence) and symmetric wedges (same isotropic impedance on the faces Z_a), the system of four coupled W-H equations reduces to the following system of equation for the E-polarization:

$$\begin{cases} \frac{\xi}{n+n_a}V_{z+}(\eta,0) = \frac{Z_a}{2}\left[I_{\rho+}(-m,-\Phi) - I_{\rho+}(-m,\Phi)\right] \\ \frac{n_a}{n+n_a}I_{\rho+}(\eta,0) = \frac{1}{2}\left[I_{\rho+}(-m,-\Phi) + I_{\rho+}(-m,\Phi)\right] \end{cases} \quad (7)$$

where $Z_a = Z_o z_a$ is the impedance of the wedge and $n_a = \omega\mu / Z_a = k\sin\vartheta_a$. Without lack of generality we analyze the properties relative to the following kernel which is related to the first equation of (7):

$$\bar{g}_1(\bar{\eta}) = \frac{\xi\, k}{z_a(n+n_a)} = \hat{g}_1(w) = -\frac{k\sin w}{z_a(\sin(w+\Phi)+1/z_a)} \quad (8)$$

Using the transformation $\bar{w} = -\pi/2 + jt$, $h_1(t) = \hat{g}_1(w)$ presents special properties along the real *t* axis which corresponds to the contour $\lambda_{\bar{w}}$. In fact this transformation creates exponential behaviors in $h_1(t)$ thus in *m(t,u)*. This spectral behavior together with the spectral behavior of the solution make the numerical evaluation of Fredholm integral equation rapidly convergent.

Fig. 4, Fig. 5 and Fig. 6 show for real *t,u* values respectively the absolute value of *m(t,u)* function, of the $y_i(u)$ function (which is the unknow function $V_{z+}(\eta,0)$ in the *u* domain [1]) and, the absolute value of *m(t,u)* times $y_i(u)$ for the impenetrable isotropic wedge at normal incidence described by eqs. (7) and (8) with the following problem parameters: kρ=10, the incident field φo=7π/12, Eo=1, Ho=0, the aperture angle Φ=3π/4, the normalized face impedance za=0.5, the integration parameters A=10, h=0.5. We observe from Fig. 6

that the dominant spectra is concentrate in *(t,u)=(0,0)* thus simple quadrature schemes with samples in this region, as the one reported in (5), are sufficient to obtain high precision numerical results.

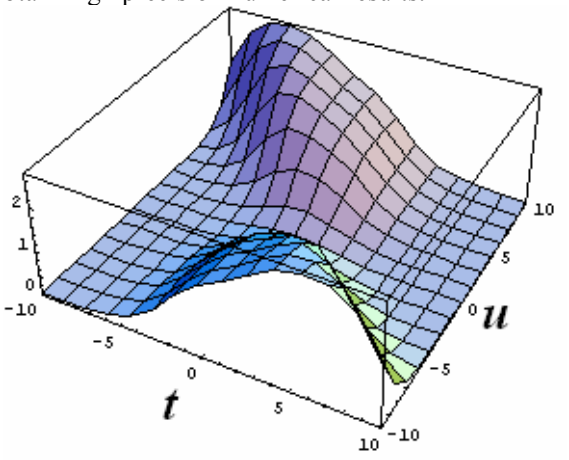

Fig. 4: The absolute value of *m(t,u)* function

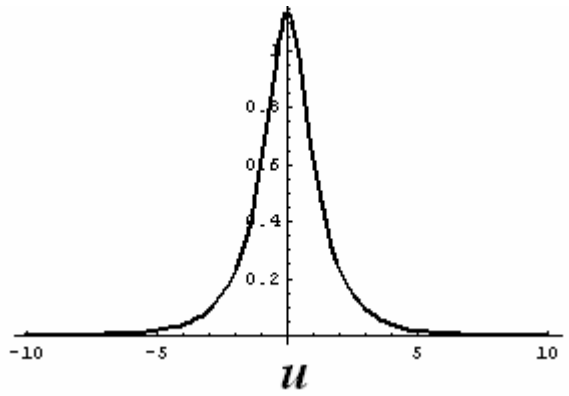

Fig. 5: The absolute value of $y_i(u)$ function

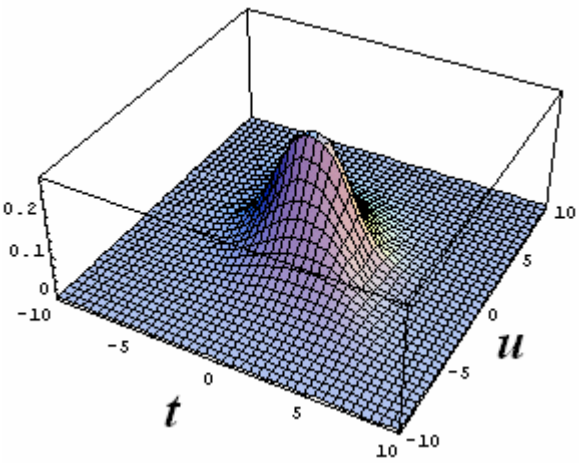

Fig. 6: The absolute value of *m(t,u)* times $y_i(u)$ function

4 NUMERICAL RESULTS

4.1 The symmetric impedance wedge at normal incidence

We have chosen, as first test case, the symmetric isotropic impedance wedge at normal incidence because the closed form solution is well known in literature using the Sommerfeld-Malyuzhinets method, see for example [2].

Fig. 7 reports the GTD Diffraction Coefficient for the test case whose parameters are reported at the end of the previous section. Besides Fig. 7 shows the GTD Diffraction Coefficient for the PEC wedge with same parameters and for the wedge problem of subsection 4.2. Peaks of the GTD Diffraction Coefficients are for φ= φo –π (incident field) and for φ= 2Φ– φo –π (reflected field). Fig. 8 reports the relative error in log10 scale of the GTD diffraction coefficient obtained through the numerical solution (using the Fredholm integral equation) and the solution obtained from the analytical procedure described below.

From eqs. (7)-(8), we factorize the scalar kernel $\bar{g}_1(\bar{\eta})$ and $\bar{g}_2(w) = \sin\vartheta_a / (\sin(w+\Phi) + \sin\vartheta_a)$ as reported below:

$$\hat{g}_{1+}(w) = \frac{\sin w}{d_\Phi(w)\sin\frac{\pi}{\Phi}w}, \quad \hat{g}_{2+}(w) = \frac{1}{d_\Phi(w)\cos\frac{\pi}{2\Phi}w} \tag{9}$$

where the special function $d_\Phi(w)$ [4] is defined by:

$$d_\Phi(w) = \exp\left[\frac{1}{\pi}\int_0^\infty \arctan\left[\frac{1}{z_a \sinh[\frac{\Phi}{\pi}u]}\right]\frac{\sinh u}{\cosh u + \cos w}du\right] \tag{10}$$

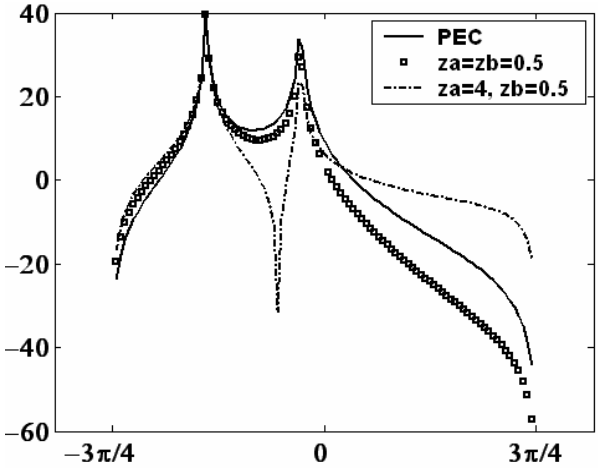

Fig. 7: GTD Diffraction Coefficient

The plus factorized $\hat{g}_{1+}(w)$ and $\hat{g}_{2+}(w)$ yields the exact solutions:

$$\hat{V}_{z+}(w,0) = -j\frac{\pi}{\Phi}\frac{\sin\frac{\pi}{\Phi}\varphi_o}{k\sin\varphi_o}\frac{\hat{g}_{1+}(-\varphi_o)}{\hat{g}_{1+}(w)}\frac{E_o}{\cos(\frac{\pi}{\Phi}w)-\cos(\frac{\pi}{\Phi}\varphi_o)} \tag{11a}$$

$$\hat{I}_{\rho+}(w,0) = j\frac{\pi}{\Phi}\frac{\sin\frac{\pi}{\Phi}\varphi_o}{kZ_o}\frac{\hat{g}_{2+}(-\varphi_o)}{\hat{g}_{2+}(w)}\frac{E_o}{\cos(\frac{\pi}{\Phi}w)-\cos(\frac{\pi}{\Phi}\varphi_o)} \tag{11b}$$

Taking into account the relationship of the special function $d_\Phi(w)$ with the Malyuzhinets function [4] yields the well known result (12) where

$n_\Phi = 2\Phi/\pi$ and $\psi(w)$ is the function defined by eq. 4.15 of [5] where $\vartheta_+ = \vartheta_- = \vartheta_a$.

$$s_E(w) = \frac{E_o}{n_\Phi} \frac{\cos[\varphi_o / n_\Phi]}{\sin[w/n_\Phi] - \sin[\varphi_o / n_\Phi]} \frac{\psi(w)}{\psi(\varphi_o)} \quad (12)$$

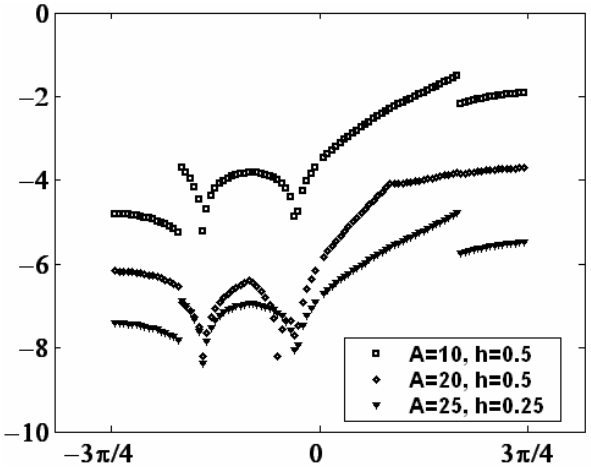

Fig. 8: Relative error in log10 scale of the GTD diffraction coefficient

4.2 The non symmetric impedance wedge at normal incidence (the Malyuzhinets problem)

We have chosen, as second test case, the non symmetric isotropic impedance wedge at normal incidence because the closed form solution is well known in literature as *the Malyuzhinets problem* [2], [5], [6].

Fig. 7 presents GTD Diffraction Coefficient and Fig. 9 presents the total field and its decomposition into the GO component and UTD component for the test case with the following parameters: kρ=10, the incident field φo=7π/12, Eo=0, Ho=1, the aperture angle Φ=3π/4, the normalized face impedance za=4, zb=0.5, the integration parameters A=10, h=0.5.

4.3 The non symmetric impedance wedge at skew incidence

Fig. 10 shows the copolar Diffraction Coefficient (we observe Ez with an Ezo incident field) for the arbitrary impenetrable wedge at skew incidence. Two different test cases are presented with the following common parameters: φo= π/2, Ezo=1, Hzo=0, Φ=7π/8, β= π /3 and A=10, h=0.5. The two test cases differ on the face impedances: 1) za=0, zb=0 (PEC wedge) and 2) za=10, zb=0.

4 CONCLUSIONS

The GWHE formulation is suitable to deal with arbitrary wedge problems with good convergence of numerical results. The procedure to obtain diffraction coefficients and total fields for anisotropic non symmetric wedge at skew incident is presented in the present paper together with the ref. [1].

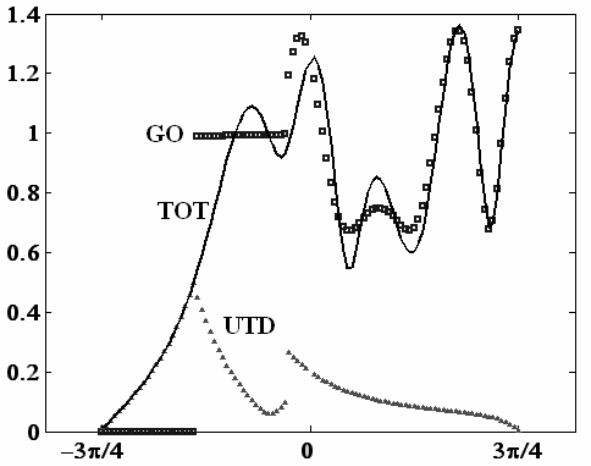

Fig. 9: Total field, GO field component and UTD field component

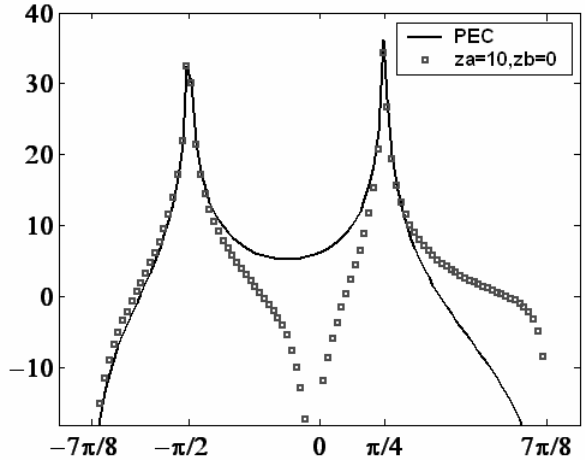

Fig. 10: The copolar GTD Diffraction Coefficient

References

[1] V. Daniele, G. Lombardi, "Wiener-Hopf formulation for wedge problems,", Proceedings of International Conference on Electromagnetics in Advanced Applications (ICEAA), Torino, September 12-16, 2005.

[2] A.N. Norris and A.V.Osipov, "Far field analysis of the Malyuzhinets solution for plane and surface waves diffraction by an impedance wedge," *Wave Motion,* vol. 30. pp. 69-89, 1999.

[3] see ref. [6] of [1].

[4] see ref [1] of [1].

[5] G. D. Malyuzhinets, "Excitation, reflection and emission of surface waves from a wedge with given face impedances," *Sov. Phys. Dokl*., vol. 3, pp. 752-755, 1958.

[6] T.B.A. Senior, J.L. Volakis, *Approximate boundary conditions in Electromagnetics,* London: The Institution of Electrical Engineers, 1995.